Spin-Echo Dynamics of a Heavy Hole in a Quantum Dot

Xiaoya Judy Wang, Stefano Chesi, and W. A. Coish

Department of Physics, McGill University, Montreal, Quebec H3A 2T8, Canada
(Received 23 August 2012; published 4 December 2012)

We develop a theory for the spin-echo dynamics of a heavy hole in a quantum dot, accounting for both hyperfine- and electric-field-induced fluctuations. We show that a moderate applied magnetic field can drive this system to a motional-averaging regime, making the hyperfine interaction ineffective as a decoherence source. Furthermore, we show that decay of the spin-echo envelope is highly sensitive to the geometry. In particular, we find a specific choice of initialization and π-pulse axes which can be used to study intrinsic hyperfine-induced hole-spin dynamics, even in systems with substantial electric-field-induced dephasing. These results point the way to designed hole-spin qubits as a robust and long-lived alternative to electron spins.

Electron spins in solid-state systems provide a versatile and potentially scalable platform for quantum information processing [1,2]. This versatility often comes at the expense of complex environmental interactions, which can destroy quantum states through decoherence. Many theoretical and experimental studies have now established that the coherence times of electron spins in quantum dots [3–6], bound to donor impurities [7,8], and at defect centers [9] are typically limited by the strong hyperfine interaction with surrounding nuclear spins [2,10]. Heavy-hole (HH) spin states in III–V semiconductor quantum dots have emerged as a platform that could mitigate the negative effects of the hyperfine interaction. Because of the p-like nature of the valence band in III–V materials, the contact interaction vanishes for hole spins, leaving only the weaker anisotropic hyperfine coupling [11,12]. Moreover, the anisotropy of this interaction in two-dimensional systems should allow for substantially longer dephasing times in a magnetic field applied transverse to the quantum-dot growth direction [10,11].

Recent experiments have measured hyperfine coupling constants for holes [13–15], as well as spin relaxation (T_1) [16] and free-induction decay times T_2^*, through indirect (frequency domain) [17] and direct (time domain) studies [18]. Coherent optical control has now been demonstrated for hole spins in single [18,19] and double quantum dots [20]. This technique has been used to implement a Hahn spin-echo sequence [18] giving an associated spin-echo decay time, $T_2 \sim 1~\mu s$. The T_2 value reported in Ref. [18] has been attributed to device-dependent electric-field fluctuations, rather than the intrinsic hyperfine interaction. Motivated by these recent experiments, here we present a theoretical study of heavy-hole spin-echo dynamics with an emphasis on identifying the optimal conditions for extending coherence times. In particular, we show that dephasing due to electric-field fluctuations, as proposed in Ref. [18], is dramatically suppressed in an alternate geometry considered here. Moreover, in contrast

with the case of electron spins, we find that hole spins can enter a motional-averaging regime in a moderate magnetic field. In this regime, coherence is no longer limited by the hyperfine interaction, solidifying the potential for long-lived hole-spin qubits.

We consider a heavy-hole spin interacting with nuclear spins in a flat quantum dot with weak strain (see Fig. 1). The HH spin is then described with the following Hamiltonian [21] (setting $\hbar = 1$):

$$H = H_Z + h_z S_z, \qquad H_Z = -\gamma_H B S_x - \sum_k \gamma_{i_k} B I_k^x, \quad (1)$$

where $\mathbf{S} = \boldsymbol{\sigma}/2$ is a pseudospin-1/2 operator in the two-dimensional ($J^z = \pm 3/2$) HH subspace and $\mathbf{I}_k$ the nuclear spin at site k. H_Z gives the hole- and nuclear-Zeeman interactions for an in-plane magnetic field $\mathbf{B} = B\hat{x}$ [see Fig. 1(a)]. γ_{i_k} is the gyromagnetic ratio of isotope i_k at site
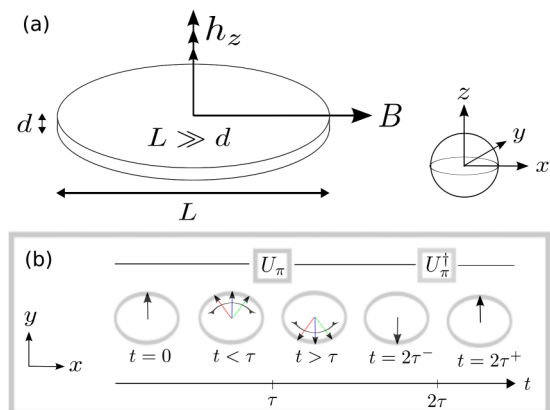

FIG. 1 (color online). (a) Quantum-dot geometry, with nuclear field h_z and magnetic field $\mathbf{B} = B\hat{x}$. For unstrained and flat quantum dots ($d \ll L$), $\gamma_H = g_\perp \mu_B \simeq 0$ and $h_{x,y} \simeq 0$ [11,22,23]. (b) Hahn-echo sequence. Two π rotations (U_π and $U_\pi^\dagger$, taken here about the x axis) are applied at $t = \tau$ and 2τ, to refocus the HH spin.

k having total spin I_{i_k}. The hole gyromagnetic ratio is $\gamma_H = g_\perp \mu_B$, with $g_\perp$ the in-plane g factor for a dot with growth axis along [001] and μ_B the Bohr magneton. The hyperfine interaction [10,11] is expressed in terms of the Overhauser operator, $\mathbf{h} = \sum_k A_k \mathbf{I}_k$. The coupling constants A_k are given by $A_k = A^{i_k} v_0 |\psi(\mathbf{r}_k)|^2$, with A^i the hyperfine constant for isotope i, v_0 the volume occupied by a single nuclear spin, and $\psi(\mathbf{r}_k)$ the HH envelope wave function. When the isotopes are distributed uniformly across the dot, we define the average $A = \sum_k A_k \simeq \sum_i \nu_i A^i$, with ν_i the isotopic abundance. In this case, and for a Gaussian envelope function in two dimensions, $A_k \simeq (A/N)e^{-k/N}$ [26], with $N = 10^4$–10^6 a typical number of nuclear spins within a quantum-dot Bohr radius. The ratio of $|A|$ to the strength of the hyperfine coupling of electrons $|A^{(e)}|$ has been estimated theoretically [11] in GaAs and confirmed experimentally [13,15] in InGaAs and InP/GaInP to be $|A/A^{(e)}| \sim 0.1$. For simplicity, we will evaluate numerical estimates with a single averaged value $|A^i| \simeq |A| \simeq 13 \mu eV$ [10,11] and ν_i, γ_i appropriate for In$_{0.5}$Ga$_{0.5}$As.

Spin echo.—Under the action of Eq. (1), spin dephasing results from fluctuations in h_z. Provided these fluctuations remain static on the time scale of decay of the hole spin, this source of decay can be removed via a Hahn echo [see Fig. 1(b)]. The process is better analyzed in the interaction picture with respect to H_Z,

$$\tilde{H}(t) = \tilde{h}_z(t)\tilde{S}_z(t), \qquad (2)$$

where, for any $\mathcal{O}$, $\tilde{\mathcal{O}}(t) = e^{iH_Z t}\mathcal{O}e^{-iH_Z t}$. In particular, $\tilde{h}_z(t) = \sum_k A_k[I_k^z \cos(\gamma_{i_k}Bt) - I_k^y \sin(\gamma_{i_k}Bt)]$ and $\tilde{S}_z(t) = [S_z \cos(\gamma_H Bt) - S_y \sin(\gamma_H Bt)]$. The time-evolution operator after a time 2τ is then given by

$$\tilde{U}(2\tau) = \mathcal{T}e^{-i\int_0^{2\tau} dt \tilde{H}_e(t)}. \qquad (3)$$

Here, $\mathcal{T}$ is the time-ordering operator and the modified echo Hamiltonian,

$$\tilde{H}_e(t) = \begin{cases} \tilde{H}(t) & 0 \le t < \tau, \\ \sigma_\alpha \tilde{H}(t)\sigma_\alpha & \tau \le t \le 2\tau, \end{cases} \qquad (4)$$

takes into account π_α pulses (π rotations about $\alpha = x, y, z$). As seen in Eq. (4), π_x pulses (but in general not π_y, π_z) have the beneficial effect of inverting the sign of the Hamiltonian, $\tilde{H}(t) \to -\tilde{H}(t)$, in the interval $\tau \le t \le 2\tau$. Provided $\tilde{H}(t)$ is approximately static over the interval $0 < t < 2\tau$, this will induce time-reversed dynamics for $\tau \le t \le 2\tau$, refocusing decay at the time 2τ. For this reason, unless otherwise specified, we will focus in the following discussion on a geometry with the magnetic field along $\hat{x}$ and π_x pulses. We will contrast this analysis later with an alternate geometry relevant to recent experiments.

Vanishing $g_\perp$.—We first consider the limit $\gamma_H = g_\perp \mu_B = 0$ in Eq. (1). The dynamics we find in this limit will be a good description whenever $\gamma_H < \gamma_i$, corresponding to $g_\perp < 10^{-3}$ ($g_\perp < 5 \times 10^{-3}$ has been reported in 2D

wells [27]). This limit considerably simplifies the theoretical analysis and allows for an exact solution: H becomes block diagonal in the eigenbasis of S_z and, in each block, the eigenstates are obtained after rotating I_k^z eigenstates by an angle $\theta_k = \pm \arctan(2\gamma_{i_k}B/A_k)$ about $\hat{y}$. Representative results of the exact evolution of $\langle S_x(2\tau) \rangle$ are shown in Fig. 2. The spin-echo signal has a remarkable dependence on the magnetic field: there is a clear transition from a low-field regime, where the decay time decreases with increasing B, to a high-field regime, where there is no decay, only modulations of the echo envelope.

To give physical insight, we have developed an analytical approximation scheme based on the Magnus expansion. The Magnus expansion is an average-Hamiltonian theory typically applied to periodic and rapidly oscillating systems [28]. This scheme is suggested by the oscillating terms in Eq. (2), and will allow us to analyze the more general problem with $\gamma_H \ne 0$. In the Magnus expansion, we assume the evolution operator, Eq. (3), can be written as $\tilde{U}(2\tau) = e^{-iH_M(2\tau)} = e^{-i\sum_{i=0}^\infty H^{(i)}(2\tau)}$. The ith-order term, $H^{(i)}(t)$, is found using standard methods [28]. Each higher-order term in the Magnus expansion contains one additional integral over time. Oscillating terms are therefore suppressed by a factor of order $\|\tilde{H}\|/\omega$, with ω the typical oscillation frequency. The leading-order term is $H^{(0)}(t) = \overline{H(t)}t$, where $\overline{H(t)}$ is simply the average of $\tilde{H}_e(t)$ over an interval t. The spin components S_α ($\alpha = x, y, z$) are then given by

$$\langle S_\alpha(2\tau) \rangle = \langle \tilde{U}^\dagger(2\tau)\tilde{S}_\alpha(2\tau)\tilde{U}(2\tau) \rangle = \langle e^{iL_M(2\tau)}\tilde{S}_\alpha(2\tau) \rangle, \quad (5)$$

where $L_M(t)$ is defined by $L_M(2\tau)\mathcal{O} = [H_M(2\tau), \mathcal{O}]$ and $\langle \mathcal{O} \rangle = \mathrm{Tr}\{\mathcal{O}\rho\}$. The initial state $\rho = \rho_S \otimes \rho_I$ is assumed to describe a product of the hole-spin (ρ_S) and nuclear-spin (ρ_I) density matrices, where the nuclear spins are in an
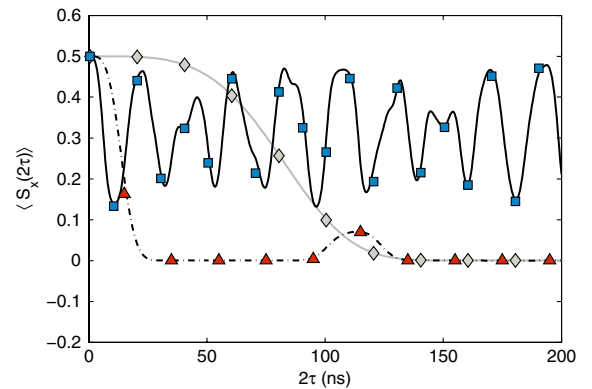

FIG. 2 (color online).   Exact analytical spin-echo decay with $B = 50$ mT (solid gray curve), $B = 2$ T (dash-dotted line), and $B = 10$ T (solid black line), corresponding to the regimes $B \lesssim A/(\gamma_i\sqrt{N})$, $B \simeq A/(\gamma_i\sqrt{N})$, and $B \gtrsim A/(\gamma_i\sqrt{N})$, respectively. Markers show the approximate form, Eq. (7). We have chosen $\langle S_x(0) \rangle = 1/2$, $N = 10^4$, $\gamma_H = g_\perp \mu_B = 0$, and γ_i from Table 1 of Ref. [10].

infinite-temperature thermal state. For $N \gg 1$ uncorrelated nuclear spins, the central-limit theorem gives nearly Gaussian fluctuations, resulting in

$$\langle e^{iL_M(2\tau)} \tilde{S}_\alpha(2\tau) \rangle \simeq \left\langle \exp\left\{ -\frac{1}{2} \langle L_M^2(2\tau) \rangle_I \right\} \tilde{S}_\alpha(2\tau) \right\rangle_S, \quad (6)$$

where we define $\langle L_M^2(t) \rangle_I \mathcal{O}_S = \mathrm{Tr}_I\{(L_M^2(t)\mathcal{O}_S)\rho_I\}$ and $\langle \mathcal{O} \rangle_S = \mathrm{Tr}_S\{\mathcal{O}\rho_S\}$.

At high B, rapid oscillations in $\tilde{H}(t)$ allow us to keep only the leading term: $L_M(2\tau)\mathcal{O}_S \simeq L^{(0)}(2\tau)\mathcal{O}_S = [H^{(0)}(2\tau), \mathcal{O}_S]$. Setting $\gamma_H = 0$, as appropriate for Fig. 2, and with the help of $\sum_k' A_k^2 \simeq \nu_i A^2/(2N)$ (where the prime restricts the sum to nuclei of isotopic species i), we obtain

$$\frac{\langle S_x(2\tau) \rangle}{\langle S_x(0) \rangle} \simeq \exp\left[-\sum_i \frac{4\nu_i A^2 I_i(I_i + 1)}{3N(\gamma_i B)^2} \sin^4\left(\frac{\gamma_i B\tau}{2}\right) \right]. \quad (7)$$

As seen in Fig. 2, Eq. (7) (markers) reproduces the exact dynamics very well. The precise conditions for the validity of the Magnus expansion will be given below.

The simple form of Eq. (7) enables us to understand why the behavior of $\langle S_x(2\tau) \rangle$ changes as B is increased. For $B \ll A/(\gamma_i\sqrt{N})$ (gray solid line in Fig. 2), a short-time expansion of Eq. (7) gives $\langle S_x(2\tau) \rangle \simeq \langle S_x(0) \rangle(1 - (\tau/\tau_0)^4) \simeq \langle S_x(0) \rangle e^{-(\tau/\tau_0)^4}$, with

$$\tau_0 \simeq \frac{1}{\sqrt{B}}\left[\sum_i \frac{\nu_i(\gamma_i A)^2}{4N} \frac{I_i(I_i + 1)}{3} \right]^{-1/4}. \quad (8)$$

Surprisingly, when B is increased, τ_0 *decreases*. This behavior is opposite to the situation for electron spins, in which the echo decay time *increases* for increasing B [29]. This decrease is due to rapid fluctuations in $\tilde{h}_z$ from nuclear spins precessing at frequencies $\sim\gamma_i B$. The Hahn echo can no longer refocus these dynamical fluctuations at finite B, although Eq. (7) does predict partial recurrences (dash-dotted line in Fig. 2) due to the finite number of discrete precession frequencies $\sim\gamma_i B$.

In contrast, at large magnetic field, $B \gtrsim A/(\gamma_i\sqrt{N})$, the system enters a motional-averaging regime in which the decay of $\langle S_x(2\tau) \rangle$ is bounded by $\sim(A/B\gamma_i\sqrt{N})^2$, giving rise to beating (black solid curve in Fig. 2). This beating has the same physical origin as electron-spin-echo envelope modulation (ESEEM) [30], although the extreme anisotropy of the hole hyperfine interaction allows uniquely for its complete suppression. Figure 3 shows the $1/e$ decay time τ_0 as B is increased, leading to a discontinuity when $\gamma_i B\sqrt{N}/A \gtrsim 1$, at which point $\langle S_x(2\tau) \rangle$ always remains close to its initial value [see Eq. (7)].

Finite $g_\perp$.—Although there are definite advantages to making flat unstrained dots leading to $g_\perp \simeq 0$ and $h_{x,y} \simeq 0$, current experiments are performed on hole systems with finite (albeit small) $g_\perp$ [18,31]. For this general case, with $\gamma_H = g_\perp \mu_B \neq 0$, we have no closed-form exact solution
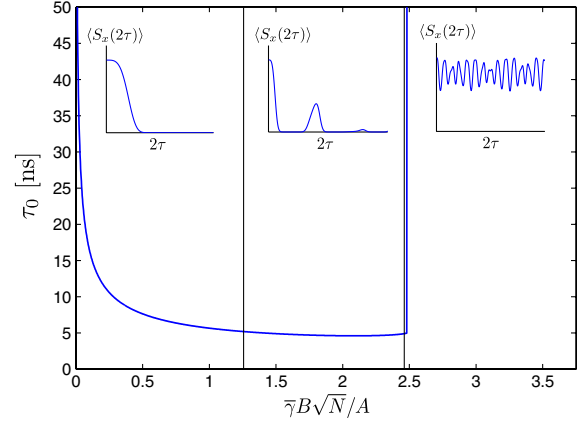

FIG. 3 (color online). Decay time τ_0 vs B. Here, $\overline{\gamma} = \sum_i \nu_i\gamma_i$ and parameters are as given in the caption of Fig. 2. Insets: Typical $\langle S_x(2\tau) \rangle$ in each of the three regions: $\overline{\gamma}B\sqrt{N}/A \ll 1$, $\overline{\gamma}B\sqrt{N}/A \sim 1$, and $\overline{\gamma}B\sqrt{N}/A \gg 1$.

for the dynamics, but our analysis can still be applied for a certain range of τ, B.

We neglect subleading oscillating terms in the Magnus expansion when $\|(H^{(0)})^2\| \gg \|H^{(0)}H^{(2)}\|$, $\|(H^{(1)})^2\|$. More specifically, if the relevant fast oscillation frequency is $\omega \sim \gamma_i B$, each precessing nuclear spin experiences a typical hyperfine field $\delta\omega_{\mathrm{rms}} \sim A/N$ from the hole. Otherwise, if the fast frequency is $\omega \sim \gamma_H B$, the hyperfine field acting on the precessing hole is of order $\delta\omega_{\mathrm{rms}} \sim A/\sqrt{N}$, averaging over the nuclear configurations. As a consequence, the parameter $\delta\omega_{\mathrm{rms}}/\omega < 1$ controls the expansion with $\delta\omega_{\mathrm{rms}}$ and ω given in Table I for each regime. In addition to bounded oscillating terms, the Magnus expansion generates terms that grow with τ. These terms approach ~ 1 at $\tau \sim \tau_{\mathrm{max}}$, beyond which a finite-order Magnus expansion may fail. Nevertheless, the Magnus expansion will provide an accurate description whenever $\delta\omega_{\mathrm{rms}}/\omega < 1$ and for $\tau \lesssim \tau_{\mathrm{max}}$. Estimates of τ_{max} are given in Table I. The sufficient conditions presented here may be overly conservative in specific cases. For example, the parameters of the $B = 50$ mT curve of Fig. 2 give a short $\tau_{\mathrm{max}} < 0.1$ ns, while the Magnus expansion is clearly valid up to a much longer time scale. This is, however, a fortuitous example; we find that in analogous calculations of free-induction decay, the bounds are tight.

In practice, the value $g_\perp = 0.04$ measured in Ref. [31] suggests that $\gamma_H \gg \gamma_i$ in many current experiments. For

TABLE I. The Magnus expansion will generally reproduce the correct dynamics for $\delta\omega_{\mathrm{rms}}/\omega < 1$ and $\tau < \tau_{\mathrm{max}}$, with ω, $\delta\omega_{\mathrm{rms}}$, and τ_{max} given below in three regimes.

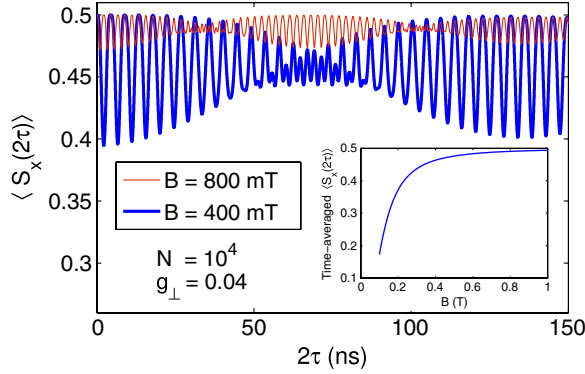|	$\gamma_H \gg \gamma_i$	$\gamma_H \ll \gamma_i < \frac{A}{B\sqrt{N}}$	$\gamma_H \ll \frac{A}{B\sqrt{N}} < \gamma_i$
ω	$\sim B\gamma_H$	$\sim B\gamma_i$	$\sim B\gamma_i$
$\delta\omega_{\mathrm{rms}}$	$\sim A/\sqrt{N}$	$\sim A/N$	$\sim A/N$
τ_{max}	$\sim \omega/\delta\omega_{\mathrm{rms}}^2$	$\sim \frac{1}{A}(\omega/\delta\omega_{\mathrm{rms}})^3$	$\sim \omega/\delta\omega_{\mathrm{rms}}^2$

FIG. 4 (color online).   Main panel: Spin-echo envelope from a
leading-order Magnus expansion when $\gamma_H \gg \gamma_i$ in the motional-
averaging regime, $\gamma_H B > A/\sqrt{N}$. Inset: Time-averaged $\langle S_x(2\tau) \rangle$.
We have taken $g_\perp = 0.04$ [31], $\langle S_x(0) \rangle = 1/2$, and $N = 10^4$.
These results are valid at least for $2\tau \lesssim 2\tau_{\max} \simeq 70$ ns(140 ns)
for $B = 400$ mT($B = 800$ mT).

$g_\perp = 0.04$, the condition $B > A/(\gamma_H \sqrt{N})$ is already satis-
fied above a rather small value, $B \gtrsim 100$ mT for $N \sim 10^4$.
In Fig. 4 we plot representative curves in this motional-
averaging regime, displaying the same features discussed
for $g_\perp = 0$. Additionally, fast oscillations at the hole
Zeeman frequency $\gamma_H B$ induce beating in the echo enve-
lope function $\langle S_x(2\tau) \rangle$, which is not present for $g_\perp = 0$.

Decay anisotropy.—While the results discussed so far
are specific to π_x pulses, other schemes are possible.
Because of the extreme anisotropy of the hole-spin hyper-
fine coupling, the spin-echo decay is also highly aniso-
tropic, depending on both the initialization and π-pulse
axes. If the hole spin is initialized along a generic in-plane
direction $\hat{n} = n_x \hat{x} + n_y \hat{y}$, and π rotations are performed
about that same axis, we find that $\langle \mathbf{S}(2\tau) \cdot \hat{n} \rangle / \langle \mathbf{S}(0) \cdot \hat{n} \rangle$ is
independent of $\hat{n}$ when $g_\perp = 0$. This result is to be
expected since any in-plane component of the hole spin
experiences the same effective field $\tilde{h}_z(t)$ along the z axis.
On the other hand, for $g_\perp \neq 0$, rotational symmetry about
the z axis is broken, resulting in a strong in-plane anisot-
ropy. For the parameters of Fig. 4, but with initialization
along $\hat{y}$ and π_x pulses, we obtain that $\langle S_y(2\tau) \rangle$ is dominated
by the hole Larmor precession about the x axis and
approaches the simple sinusoidal function $\langle S_y(2\tau) \rangle \simeq
\langle S_y(0) \rangle \cos(2\gamma_H B\tau)$ in the motional-averaging regime,
$\gamma_H B > A/\sqrt{N}$.

Additional dephasing mechanisms other than the nu-
clear bath can also have a strong influence on the preces-
sion about $\hat{x}$, introducing other sources of anisotropy. In
particular, the decay of $\langle S_y(2\tau) \rangle$ was measured in Ref. [18]
with π_z pulses used for the Hahn echo. The resulting decay
was found to be approximately exponential, $\langle S_y(2\tau) \rangle \simeq
\langle S_y(0) \rangle e^{-2\tau/T_2}$, with a B-independent $T_2 \sim 1\ \mu$s. This
behavior was attributed to spectral diffusion induced by
electric-field noise, which we model here by setting

$\gamma_H B \to \gamma_H B + \delta\omega(t)$ in Eq. (1). The observed exponen-
tial decay is consistent with Gaussian white noise
[32] $\langle \delta\omega(t)\delta\omega(t') \rangle_{\delta\omega} = \frac{2}{T_2} \delta(t - t')$ [and $\langle \delta\omega(t) \rangle_{\delta\omega} = 0$],
where $\langle \cdots \rangle_{\delta\omega}$ indicates averaging with respect to realiza-
tions of $\delta\omega(t)$. We have included this additional dephasing
mechanism in the evaluation of Eq. (6) for the π_x-pulse
echo sequence examined previously and obtained a power-
law decay at $\tau \gg T_2$:

$$\frac{\langle S_x(2\tau) \rangle}{\langle S_x(0) \rangle} \simeq \left\langle \exp\left[\frac{\langle h_z^2 \rangle_I}{2} \sum_{\alpha=y,z} f_\alpha^2(t) \right] \right\rangle_{\delta\omega} \simeq \frac{1}{1 + \tau/\tau_D}, \quad (9)$$

where $f_y(\tau) = \int_0^{2\tau} \sin\phi(t)\text{sgn}(\tau - t)dt$, $f_z(\tau) =
\int_0^{2\tau} \cos\phi(t)dt$, $\phi(t) = \gamma_H Bt + \int_0^t \delta\omega(t')dt'$, and

$$\tau_D = \frac{1 + (\gamma_H BT_2)^2}{2\langle h_z^2 \rangle_I T_2}. \quad (10)$$

This decay time scale is exceedingly long ($\tau_D \simeq 20$ s)
for the experimental value $\gamma_H B \simeq 2 \times 10^{11}$ s^{-1} and using
$\langle h_z^2 \rangle_I \sim 10^{15}$ s^{-2}, which demonstrates the negligible effect of
spectral diffusion on the previous discussion (e.g., Figs. 2–4).
For simplicity, we have derived Eqs. (9) and (10) with static
nuclear-field fluctuations $\langle h_z^2 \rangle_I$. This corresponds to a worst-
case scenario for the present model. At the high magnetic field
of Ref. [18] ($B \sim 8$ T), motional averaging would likely
inhibit decay even further.

Conclusion.—We have calculated the spin-echo dynam-
ics of a single heavy-hole spin in a flat unstrained quantum
dot. The relevant dynamics are highly anisotropic in the
spin components and π-rotation axes. When $\gamma_H \ll \gamma_i$, we
predict an initial decrease of the coherence time with
increasing B, followed by a complete refocusing of the
HH-spin signal and motional averaging when $B \gtrsim B_c$
($B_c \sim A/\gamma_i\sqrt{N} \simeq 3$ T for $N = 10^4$). The motional-
averaging regime is also realized when $\gamma_H \gg \gamma_i$, relevant
to current experiments. In this regime, decay due to the
hyperfine coupling can only occur for $\tau \gtrsim \tau_{\max} \propto B$, and
can therefore be completely suppressed. We have further
shown that device-dependent electric-field noise becomes
negligible for a specific geometry, allowing for a measure-
ment of the limiting intrinsic decoherence due to nuclear
spins. We expect the systematic approximation scheme
introduced here to find wide applicability to a number of
other challenging spin dynamics problems associated with
nitrogen vacancy centers, donor impurities, and electrons
in quantum dots.

[1] D. Loss and D. P. DiVincenzo, Phys. Rev. A **57**, 120
    (1998).
[2] R. Hanson, L. P. Kouwenhoven, J. R. Petta, S. Tarucha,
    and L. M. K. Vandersypen, Rev. Mod. Phys. **79**, 1217
    (2007).

[3] A. V. Khaetskii, D. Loss, and L. Glazman, Phys. Rev. Lett. **88**, 186802 (2002).

[4] I. A. Merkulov, A. L. Efros, and M. Rosen, Phys. Rev. B **65**, 205309 (2002).

[5] J. Petta, A. Johnson, J. Taylor, E. Laird, A. Yacoby, M. Lukin, C. Marcus, M. Hanson, and A. Gossard, Science **309**, 2180 (2005).

[6] H. Bluhm, S. Foletti, I. Neder, M. Rudner, D. Mahalu, V. Umansky, and A. Yacoby, Nat. Phys. **7**, 109 (2010).

[7] R. de Sousa and S. Das Sarma, Phys. Rev. B **68**, 115322 (2003).

[8] R. E. George, W. Witzel, H. Riemann, N. V. Abrosimov, N. Nötzel, M. L. W. Thewalt, and J. J. L. Morton, Phys. Rev. Lett. **105**, 067601 (2010).

[9] L. Childress, M. Dutt, J. Taylor, A. Zibrov, F. Jelezko, J. Wrachtrup, P. Hemmer, and M. Lukin, Science **314**, 281 (2006).

[10] W. A. Coish and J. Baugh, Phys. Status Solidi B **246**, 2203 (2009).

[11] J. Fischer, W. A. Coish, D. V. Bulaev, and D. Loss, Phys. Rev. B **78**, 155329 (2008).

[12] B. Eble, C. Testelin, P. Desfonds, F. Bernardot, A. Balocchi, T. Amand, A. Miard, A. Lemaitre, X. Marie, and M. Chamarro, Phys. Rev. Lett. **102**, 146601 (2009).

[13] E. A. Chekhovich, A. B. Krysa, M. S. Skolnick, and A. I. Tartakovskii, Phys. Rev. Lett. **106**, 027402 (2011).

[14] E. A. Chekhovich, A. B. Krysa, M. Hopkinson, P. Senellart, A. Lemaitre, M. S. Skolnick, and A. I. Tartakovskii, arXiv:1109.0733.

[15] P. Fallahi, S. T. Yilmaz, and A. Imamoglu, Phys. Rev. Lett. **105**, 257402 (2010).

[16] B. Gerardot, D. Brunner, P. Dalgarno, P. Ohberg, S. Seidl, M. Kroner, K. Karrai, N. Stoltz, P. Petroff, and R. Warburton, Nature (London) **451**, 441 (2008).

[17] D. Brunner, B. D. Gerardot, P. A. Dalgarno, G. Wüst, K. Karrai, N. G. Stoltz, P. M. Petroff, and R. J. Warburton, Science **325**, 70 (2009).

[18] K. De Greve, P. McMahon, D. Press, T. Ladd, D. Bisping, C. Schneider, M. Kamp, L. Worschech, S. Hoefling, A. Forchel, and Y. Yamamoto, Nat. Phys. **7**, 872 (2011).

[19] T. M. Godden, J. H. Quilter, A. J. Ramsay, Y. W. Wu, P. Brereton, S. J. Boyle, I. J. Luxmoore, J. Puebla-Nunez, A. M. Fox, and M. S. Skolnick, Phys. Rev. Lett. **108**, 017402 (2012).

[20] A. Greilich, S. G. Carter, D. Kim, A. S. Bracker, and D. Gammon, Nat. Photonics **5**, 702 (2011).

[21] In Eq. (1), we neglect terms $\sim h_{x,y}$, and nuclear quadrupole coupling. This is valid for a flat quantum dot with weak strain [11,22–24]. The nuclear dipolar interaction may also influence the Hahn-echo decay of an electron spin on a time scale $\tau_{dd} \sim 10~\mu s \propto 1/\sqrt{A^{(e)}}$ [25]. Since $|A| < |A^e|$, we expect τ_{dd} to be still longer for holes, beyond the times considered here.

[22] J. Fischer and D. Loss, Phys. Rev. Lett. **105**, 266603 (2010).

[23] F. Maier and D. Loss, Phys. Rev. B **85**, 195323 (2012).

[24] N. A. Sinitsyn, Y. Li, S. Crooker, A. Saxena, and D. L. Smith, Phys. Rev. Lett. **109**, 166605 (2012).

[25] W. Yao, R.-B. Liu, and L. J. Sham, Phys. Rev. B **74**, 195301 (2006).

[26] W. A. Coish and D. Loss, Phys. Rev. B **70**, 195340 (2004).

[27] T. Korn, M. Kugler, M. Griesbeck, R. Schulz, A. Wagner, M. Hirmer, C. Gerl, D. Schuh, W. Wegscheider, and C. Schüller, New J. Phys. **12**, 043003 (2010).

[28] M. M. Maricq, Phys. Rev. B **25**, 6622 (1982).

[29] L. Cywiński, W. M. Witzel, and S. Das Sarma, Phys. Rev. Lett. **102**, 057601 (2009).

[30] L. G. Rowan, E. L. Hahn, and W. B. Mims, Phys. Rev. **137**, A61 (1965).

[31] X. Marie, T. Amand, P. Le Jeune, M. Paillard, P. Renucci, L. E. Golub, V. D. Dymnikov, and E. L. Ivchenko, Phys. Rev. B **60**, 5811 (1999).

[32] J. R. Klauder and P. W. Anderson, Phys. Rev. **125**, 912 (1962).